Journal of Green Energy Research and Innovation

Improving the Maximum Power Point Tracking in a Photovoltaic System Based on the Resistance-Predictive Method

Moaiad Mohseni, Alireza Niknam Kumleh, Mehdi Alibakhshi, Mona Sheikhi Abou Masoudi

Highlight

- Enhancing the MPPT by designing and controlling the step-up converter of the PV system
- Ensuring an efficient MPPT by proper calculation of parameters
- Employing predictive control to enhance the speed of MOSFET switching decisions
- Implementing a resistive-predictive step-up converter control

Graphical Abstract

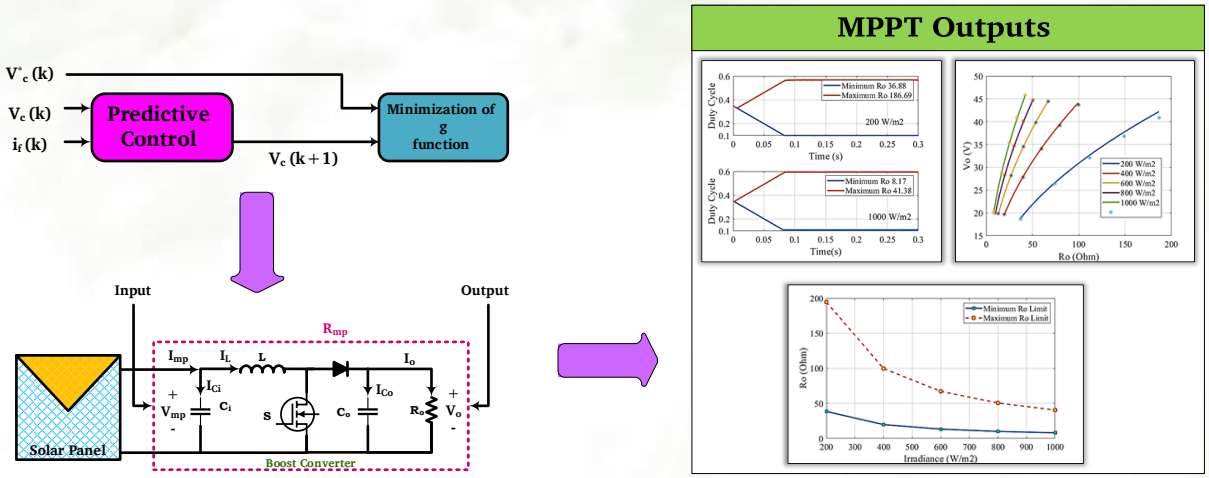

Use your device to scan and read the article online

Citation

M. Mohseni, A. Niknam Kumleh, M. Alibakhshi, and M. Sheikhi Abou Masoudi, "Improving the Maximum Power Point Tracking in a Photovoltaic System Based on the Resistance-Predictive Method," *Journal of Green Energy Research and Innovation*, vol. 1, no. 2, pp. 81-102, 2024.

https://doi.org/10.61186/jgeri.1.2.81

JGERI Journal of Green Energy Research and Innovation

Online ISSN: 3041-9018

Journal of Green Energy Research and Innovation

Journal Homepage: www.jgeri.araku.ac.ir

Improving the Maximum Power Point Tracking in a Photovoltaic System Based on the Resistance-Predictive Method

Moaiad Mohseni [1]*, Alireza Niknam Kumleh [2], Mehdi Alibakhshi [3], Mona Sheikhi Abou Masoudi [4]

[1] *Khuzestan Regional Electric Company, Ahvaz, Iran.*
[2] *Faculty of Electrical Engineering, Amirkabir University of Technology (Tehran polytechnic), Tehran, Iran.*
[3] *Department of Electrical Engineering, Islamic Azad University of Tehran, Tehran, Iran.*
[3] *Department of Electrical Engineering, Naghshejahan Institute of Higher Education, Baharestan, Isfahan, Iran.*

* *Corresponding Author: moaiadmohsenii@gmail.com*

ARTICLE INFO

Keywords:
Boost converter,
Enhancement of MPPT,
Predictive method,
PV system,
Resistance method.

Article history:
Received: 27 January 2024;
Revised: 27 February 2024;
Accepted: 01 March 2024;

Article type:
Research Article

ABSTRACT

An established technique to maximize the output power of photovoltaic (PV) systems, thereby raising the efficiency of renewable energy systems, is maximum power point tracking (MPPT). This paper focuses on designing and controlling a boost converter for MPPT in a PV system to calculate the appropriate range of output resistance, minimum inductance, input capacitor, and output capacitor for the boost converter so that the maximum PV output is achieved and the decision speed of MOSFET switching is obtained by adopting the combined resistance-predictive method. The simulation results demonstrate the efficacy of the proposed method in attaining these objectives. The suggested technique can effectively track the maximum power point (MPP) within a broad spectrum of solar radiation while ensuring that the duty cycle remains within its permissible range.

1. Introduction

1.1. Research Motivation

Solar power will remain a renewable and sustainable energy source because of its superior environmental friendliness and abundant availability. Maximum power point tracking (MPPT) is a technique employed in solar power systems to optimize the extraction of electricity from photovoltaic (PV) modules, which is achieved by closely monitoring the operational state of the modules. To optimize the electricity output from a solar panel, it is essential to use MPPT, particularly in situations where the weather conditions are uncertain [1]. In order to mitigate global warming, it is imperative to substitute hydrocarbon deposit systems with renewable energy sources, such as the sun and wind [2]. To enhance the efficiency of renewable energy systems, PV systems are equipped with an MPPT algorithm to ensure that each module operates at its optimal power point [3]. PV cells exhibit a voltage-current curve that accurately represents their operational state. The maximum power point (MPP) of this curve occurs when the cell generates the highest amount of power to be delivered to a load. The cellular function is

diminished when it is not operational. This paper focuses on the layout and manipulation of a boost converter for MPPT in a PV device. The intention is to calculate the best variety of output resistance, minimal inductance, input capacitor, and output capacitor for the boost converter so that the maximum PV output is achieved and the decision pace of MOSFET switching is obtained by adopting the combined resistance-predictive approach.

1.2. Literature review

There are straightforward techniques to achieve optimal power output in both conventional and dynamic shading scenarios. The MPPT method has been designed to optimize the power output of a solar panel system in the presence of partial shadowing [4]. The topics of discussion in [5] included energy storage, solar production, and optimization of production system dimensioning with storage. Grid-connected PV systems are sized according to the selection of modules, DC/AC inverters, and auxiliary equipment [5]. Reference [6] presents the application of particle swarm optimization (PSO) to maximize the highest power output of PV systems. It also aims to identify the most effective design variable for penalizing the step size of two conventional methods. The authors in [7] propose a bionic two-stage MPPT control method to enhance the precision and speed of the MPPT process. The strategy consists of a fast-positioning stage and a precise determination step, which optimize the duty cycle of the DC-DC converter. The authors in [8] propose a new method to maximize the power output of a PV system by using the Horse Herd Optimization (HHO) algorithm in various weather circumstances. Fault analysis and protection of distributed generations, such as PVs and wind turbines, are also a concern of academia and have been addressed in [9] even though there is a research gap concerning comprehensive work on the protection of PV cells [10].

References [11] and [12] have carefully analyzed the reactions and the electricity production process, accounting for most reasons for changing the behavior of solar panels against weather fluctuations based on the amount of received photon energy and describing the amount of energy gap between the p and n junctions of the semiconductors inside the panel. The most basic model of a PV that has a diode is obtained from these references. The simplest configuration of a PV system incorporating a diode can be derived from these sources. Reference [13] introduces a sophisticated software package that efficiently determines the ideal capacity of PV systems for the electrification of remote and rural areas. The software addresses the challenge of minimizing transportation, electrification, and maintenance expenses. Reference [14] presents a model aimed at optimizing smart homes to enhance the efficiency and reduce energy consumption of electricity generated by PV systems. The outputs of this model will include establishing the composition of walls and windows, calculating the ideal size of panels, and identifying the most suitable location for them. The researchers in [15] developed systems with numerous PVs exhibiting distinct characteristic curves. The primary objective was to ascertain the precise elevation, angle of inclination towards solar radiation, and the most favorable placement for each panel. The full-bridge cascade converter is an inverter widely used in PV systems. It was specifically designed in [16] to

be more robust than its previous versions, offering increased reliability, reduced switching losses, improved efficiency, enhanced short-circuit fault capability, and greater stability in the face of extreme weather fluctuations. Boost converters are extensively employed in PV systems and have seen the development and implementation of multiple structures. The structure described in [17] utilizes a parallel input (parallel input inductors)-series output (series output capacitors) configuration, which has demonstrated excellent efficacy in mitigating current ripple. In addition, the converter proposed in [18] does not require a transformer and possesses the inherent capability to evenly distribute the power obtained from PV arrays. This converter operates with an input voltage of 24 V and outputs a voltage of 100 V at a frequency of 100 kHz. It is specifically built to handle a nominal power of 60 W. Reference [19] presents the design and construction of a multi-level inverter that connects PV arrays to the grid. This inverter has a modular and extendable structure and allows for adding a stabilizer to each panel. The PV units with numerous panels are typically categorized into two types of equivalent circuits: a) single-unit models and b) multi-unit models. In the former type, all panels are treated as a complete unit connected to the grid via a single transformer and impedance. This approach necessitates a few computations and has garnered recommendations from numerous international standard organizations. However, when the panels are situated in significantly distinct geographical locations, this technique exhibits a pretty substantial margin of error, rendering it not advisable [20]. The concept of categorizing PV panels into various clusters is introduced in multi-unit models. Each cluster is represented by an equivalent PV unit, which consists of a complete panel, an equivalent impedance, and a comprehensive transformer. In this approach, the PVs in each cluster are assumed to be almost identical, with any minor variations being disregarded. Given the exceptional precision of multi-unit models, this approach is widely employed in numerous simulation studies and analyses of grid-connected solar power facilities. The single-unit model is a distinct type of multi-unit model [21].

Typically, three models have been proposed for solar cells, including the single-diode, two-diode, and multi-diode models. The single-diode model has the fewest physical parameters. As a result, it has widely been employed in numerous studies to depict the voltage-current characteristics of cells using only four or five parameters. This model is highly cost-effective in terms of mathematical and computational resources, but its precision is contingent upon the specific solar cell technology employed. Several studies indicate that this model exhibits a slight bias towards optimism when predicting the behavior of the cell, as it incorporates a higher proportion of solar energy from the sun in its calculations. However, the actual output of the solar cell is lower than the values obtained from these calculations [22]. The two-diode model is a modified version of the single-diode model that distinguishes between two distinct operating modes of the solar cell: the high-voltage mode and the low-voltage mode. The high-voltage mode of this model is identical to the single-diode mode. However, the low-voltage mode is simulated using a separate diode, and the impact of recombination within the solar cell is considered. The two-diode approach is highly appropriate for situations characterized by low levels

of solar radiation or low ambient temperatures. Consequently, it yields more precise outcomes regarding the performance of the solar cell under low radiation situations [23]. The multi-diode model has superior accuracy compared to alternative models, effectively capturing the solar cell's performance throughout varying temperature conditions and radiation levels. This model requires access to diverse facts that must be precisely characterized by measurement under varied conditions, and these items are not readily accessible in several information sheets. This model exhibits a significant computational burden and is not time-efficient, but it has yielded highly favorable outcomes in numerous solar cells [24].

The peak power and voltage levels are not constant and vary in response to temperature and the angle of sun exposure. By monitoring the power output, the PV system can achieve its highest level of efficiency, resulting in reduced operational costs. There exist numerous variations of MPPT methods, typically categorized into two groups: conventional approaches and novel methods relying on computational algorithms [25]. The soft computing-based methods are novel MPPT approaches that encompass the following techniques: a) fuzzy logic control, b) artificial neural network method, c) adaptive neural fuzzy methods, and d) metaheuristic algorithms, such as genetics and differential evolution [26]. Multiple concerns have been identified in the design of the MPP tracker converter. A subject discussed is the investigation of the link between the equivalent resistance of the PV cell, the output resistance of the converter, and its duty cycle. This analysis, referenced as [27], aims to identify the most efficient converter for connecting the solar cell to the load. The design of the MPP tracker converter, as described in reference [28], represents the power electronic converter as a variable resistance. However, the equivalent impedance of the power electronic converter does not include an inductor or capacitor. The MPP tracker converter has traditionally been designed using conventional methods for DC-DC converters connected to voltage sources [29]. However, it is important to note that the solar cell, being fundamentally nonlinear, cannot be regarded as a linear power supply. Hence, this approach will not yield accurate outcomes. Another approach employed in the design of the MPP tracker converter involves the utilization of small-signal analysis [30]. Nonetheless, this analysis does not encompass the function of the inductor and capacitor in the converter. So, it is unfeasible to compute the inductor and capacitor of the converter using this approach. The calculations pertaining to the design of the inductor and capacitor for the MPP tracker converter are available in [31]. The operation mode of the boost converter has always taken into account continuous current, assuming optimum weather conditions. Reference [32] designed a maximum power tracker buck converter operated based on the predictive model control approach. The proposed power point tracking method is the internal inductance method, which is used as the reference signal of the predictive control model. This optimization technique, which is available online, predicts the current and future condition of the system. This strategy has the benefit of a fast transient response and the elimination of disturbances, in contrast to conventional methods.

The authors in [33] presented an MPP tracker boost converter with a maximum power detector. This converter utilizes a mix of perturbation and observation (P&O) method together with the predictive model control method. Simply put, the predictive control system utilizes the MPP as its reference signal. The impact of altering the step size of the tracking method has also been subjected to sensitivity analysis. This strategy offers the benefit of eliminating any instances of overshoots and undershoots that are associated with switching. Reference [34] discusses the incorporation of the P&O MPPT and the prediction model control methods. This method has been implemented in a boost converter that is coupled to a solar cell. The speed of this method in achieving the MPP has been enhanced, and its capacity to control voltage has been boosted as well. The impact of variations in irradiation and ambient temperature on the suggested method has been examined, and the method has been successfully deployed in real-time. References [35-37] introduce a resilient controller for accurately tracking the MPP of a single-phase multilevel inverter. This is achieved by the use of a predictive control model, resulting in enhanced P&O techniques. Previous methods have been surpassed in efficiency and speed of the control loop, resulting in reduced switching losses as well.

1.3. The significance of research

Given the expansion of PV technology, its efficient operation is crucial both technically and economically. Furthermore, it is crucial to develop models for converters with the objective of MPPT from a scientific and research perspective. The adoption of predictive control approaches also enables the industrialization of these techniques. This paper aims to enhance MPPT by designing and controlling the step-up converter of the PV system. The range of output resistance, minimum inductance, input capacitor, and output capacitor for the boost converter are calculated to ensure efficient MPPT. Predictive control is employed to enhance the speed of MOSFET switching decisions. The study introduces a novel approach to enhancing the MPPT in a PV system by implementing a resistive-predictive step-up converter control.

1.4. Novelty and main contributions

The novelty of the research lies in calculating the ideal range of output resistance, minimal inductance, input capacitor, and output capacitor for the boost converters so that the maximum PV output is executed and the selection speed of MOSFET switching is received by means of adopting a mixed resistance-predictive method.

The remaining of the paper is as follows. Section 2 describes the suggested model, while Section 3 provides a detailed explanation of the program execution algorithm and Section 4 provides the details of the implementation of simulations.

2. Materials and Approaches

This section first presents the equations related to the solar cell model, its technical specifications, and the topology of the MPP tracker converter. Then, the hill climbing (HC) tracking method is studied, and based on the concept of the predictive control model method, the combination of these two methods is implemented in MPPT.

2.1. PV cell model

As the primary source of energy production in PV systems, the solar cell is of particular importance. The importance of its modeling and the types of models available for it were briefly discussed. This study used the most common and simplest solar cell model, called the single-diode model. It should be noted that this model is mostly used in medium and acceptable levels of irradiation and is not very suitable for applications with poor irradiation. Therefore, a simplifying assumption is to consider the appropriate radiation in the studied time period. If more in-depth studies are needed, two-diode or multi-diode models are recommended to be considered. The equivalent circuit diagram of a single-diode solar cell is shown in Figure 1.

Currents I_{ph}, I_s, and I_{PV} represent the flow of photons, the dark saturation current, and the output current of the cell, respectively. Also, the series and shunt resistance of the cell are represented by R_s and R_{sh}, respectively. As is known, the relationship between the PV voltage and the current is not linear due to the presence of the diode. Using the KVL laws, the relationship between the voltage and current of the PV cell [31,38] is represented by Equation (1):

$$I_{PV} = I_{ph} - I_s\left(e^{\frac{(V_{PV}-I_{PV}R_s)}{AV_T}} - 1\right) - \frac{(V_{PV} - I_{PV}R_s)}{R_{sh}} \quad (1)$$

where V_T is the thermal voltage obtained based on Boltzmann's constant, the temperature of the p-n junction, and the electric charge of the electron according to Equation (2):

$$V_T = \frac{kT}{q} \quad (2)$$

For each voltage, Equation (3) must be solved to reach the current-voltage characteristic curve of a PV. In this equation, the photon current shows the dependence of the problem on solar radiation. The dark saturation current also shows the dependence of the equation on the ambient temperature. The MPP is usually obtained by adjusting two series and shunt resistors. The calculation of photon currents and dark saturation is obtained based on the information in the datasheet of each solar cell based on Equations (2) and (3) [21, 31]:

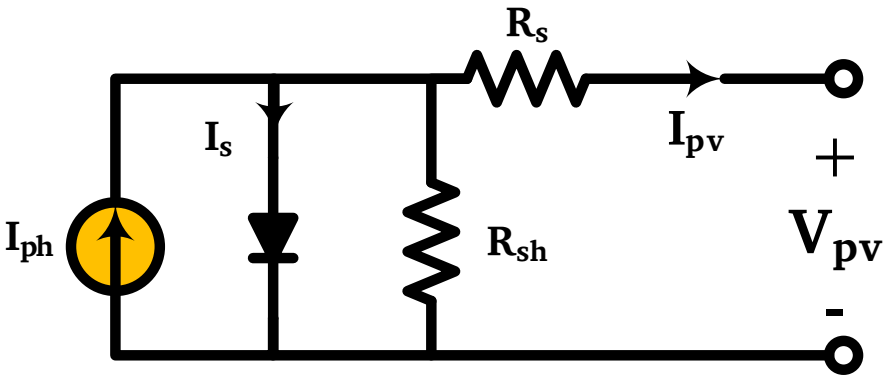

Figure 1. The single-diode model of a PV cell [21].

$$I_{ph} = \frac{G}{G_{stc}}(I_{stc} + K_i(T - T_{stc}) \quad (3)$$

$$I_s = \frac{I_{sc} + K_i(T - T_{stc})}{e\left(V_{oc} + \frac{k_v(T - T_{stc})}{AV_T}\right) - 1} \quad (4)$$

where G is the solar radiation, STC shows the standard test conditions, G_{stc} is the radiation in standard conditions, K_i denotes the temperature coefficient of short-circuit current, T_{stc} is the temperature in standard conditions, and k_v expresses the temperature coefficient in open-circuit voltage.

Based on the characteristic curve of solar cells, the voltage-to-current ratio of the cell can be observed at the operating point of maximum power, and by dividing the cell voltage by its current, the equivalent resistance of the circuit can be obtained from the point of view of the solar cell. If there is no change in the amount of solar radiation or temperature conditions, this value will remain almost constant. Therefore, the equivalent resistance from the PV point of view at the maximum power operating point will be given by Equation (5):

$$R_{mp} = \frac{V_{mp}}{I_{mp}} \quad (5)$$

Since it is possible to use PVs in different radiations and temperatures, the resistance equivalent of the MPP must be obtained over a range of radiations. Also, a range for the minimum and maximum values of resistance equivalent to MPP should be considered so that the design of the boost converter can have an acceptable efficiency.

2.2. Circuit analysis of an ideal boost converter for MPPT purposes

The circuit schematic of an MPP tracker boost converter is shown in Figure 2. As shown, the input side of the converter is connected to the solar cell, and the other side is connected to the load. If the boost converter is assumed to be ideal, i.e., no losses are considered for switching this converter, based on the law of energy conservation, it can be said that the input power of the converter is equal to its output power, so it can be written as Equation (6) [31]:

$$P_{input} = P_{output} \rightarrow \frac{V^2{}_{mp}}{R_{mp}} = \frac{V^2{}_o}{R_o} \quad (6)$$

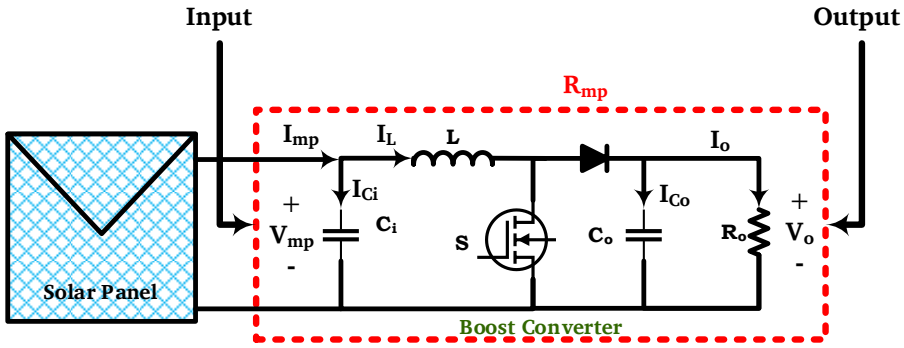

Figure 2. Circuit schematic of a boost converter for MPPT purposes [31].

Because the purpose is the operation and control of the boost converter in the continuous current area, a linear relationship is established between the input and output voltage of the boost converter based on the duty cycle, as given in Equation (7):

$$V_o = \frac{V_{mp}}{1 - D} \tag{7}$$

Therefore, by replacing Equation (7) in Equation (6), the relationship given in Equation (8) is obtained.

$$R_o = \frac{R_{mp}}{(1 - D)^2} \tag{8}$$

The required duty cycle of the boost converter control is provided in Equation (9).

$$R_o = \frac{R_{mp}}{(1 - D)^2} \tag{9}$$

Therefore, the duty cycle is somehow dependent on the relationship between the equivalent resistance of the solar cell and the output resistance of the boost converter and is determined based on its ratio.

2.2.1. Determining the range of output resistor

It is assumed that the radiation is at its lowest permissible limit. In other words, it is placed at the highest value of its permissible range. In such a situation, the duty cycle can also change from D_{min} to D_{max} as its allowed value. In this case, the minimum and maximum values of the output resistance are obtained nu Equations (10) and (11), respectively [34]:

$$R_o^{min} = \frac{R_{mp}^{max}}{(1 - D_{min})^2} \tag{10}$$

$$R_o^{max} = \frac{R_{mp}^{max}}{(1 - D_{max})^2} \tag{11}$$

On the other hand, assume that the solar radiation is at its maximum value; that is, R_{mp} is at the lowest value of its allowed range, i.e., R_{mp}^{min}. In such a situation, the duty cycle can also change from D_{min} to its allowed value of D_{max}. In this case, the minimum and maximum values of the output resistance are calculated by Equations (12) and (13), respectively:

$$R_o^{min} = \frac{R_{mp}^{min}}{(1 - D_{min})^2} \tag{12}$$

$$R_o^{max} = \frac{R_{mp}^{min}}{(1 - D_{max})^2} \tag{13}$$

2.2.2. Sizing the inductance

According to Figure 2, when the power switch is closed (when the switch is on), the inductor starts charging and the voltage of the two ends of the solar cell is placed in the

two ends of the inductor ($V_L = V_{mp}$). The turn-on duration of the switch is also $\Delta t = DT_s$s. Therefore, the current of the inductor starts to increase from its initial value, and the value of this increase based on the relationship between the voltage and current of the inductor (Faraday's law) will be equal to Equation (14):

$$V_L = L\frac{\Delta i_L}{\Delta t} \rightarrow \Delta i_L = \frac{DT_s}{L}V_{mp} = \frac{D}{f_s L}V_{mp} \tag{14}$$

Equation (14) determines the ripple value of the inductor current. On the other hand, since the average current passing through the capacitors is equal to zero, the average current of the inductor will be equal to the average current of the solar cell, so Equation (15) is established:

$$I_L = I_{mp} \tag{15}$$

The boundary between discrete and continuous operation is when the current ripple $\boldsymbol{\Delta i_L}$is equal to the average current of the inductor $\boldsymbol{I_L}$. So, Equation (16) is established as follows:

$$I_L = \Delta i_L \rightarrow I_{mp} = \frac{DT_s}{I_{mp}}V_{mp} \rightarrow L = \frac{DT_s}{I_{mp}}V_{mp} \rightarrow L = \frac{D}{f}\frac{V_{mp}}{I_{mp}} \tag{16}$$

As it is known, the value of the inductor in the critical state can be determined based on the voltage and current of the maximum power point of the cell. The ratio $\frac{\boldsymbol{V_{mp}}}{\boldsymbol{I_{mp}}}$ is the same equivalent resistance ($\boldsymbol{R_{mp}}$) of the solar cell. Therefore, we can have [33]:

$$L = \frac{D}{f_s}R_{mp} \rightarrow L = \left(1 - \sqrt{\frac{R_{mp}}{R_o}}\right)\left(\frac{R_{mp}}{f_s}\right) \tag{17}$$

According to Equation (17), it can be said that determining the inductor value is a function of three parameters: solar cell resistance, switching frequency, output resistance, and duty cycle. To better understand, Figure 3 shows the depiction of the two equations given in Equation (17).

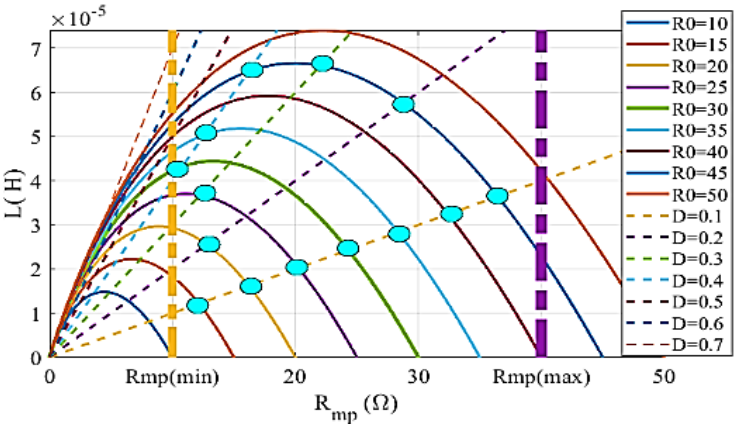

Figure 3. Inductance value based on solar cell resistance, output resistance, and duty cycle [33].

Figure 3 shows the relationship between the inductor and the resistance of the solar cell in different output resistances, and the lines with constant slopes represent the same relationship but in different duty cycles. From the intersection of these curves, the required inductor values of the boost converter are determined. The lowest allowed value for L is when the resistance of the solar cell and the diode cycle are at their minimum. So, we will have Equation (18):

$$L_{min} = \frac{D_{min}}{f_s} R_{mp}^{min} = \left(1 - \sqrt{\frac{R_{mp}}{R_o}}\right) \frac{R_{mp}}{f_s} \tag{18}$$

The peak point of the curves in Figure 3 can be obtained by differentiation of Equation (17). If it is assumed that R_o is constant, then by differentiating Equation (17) with respect to the variable R_{mp} and setting it to zero, we will have Equation (19):

$$\frac{dL}{dR_{mp}} = \frac{d}{dR_{mp}}\left(1 - \sqrt{\frac{R_{mp}}{R_o}}\right)\frac{R_{mp}}{f_s} + \left(1 - \sqrt{\frac{R_{mp}}{R_o}}\right)\frac{d}{dR_{mp}}\left(\frac{R_{mp}}{f_s}\right) \tag{19}$$

By applying derivation and simplifying the results, Equation (20) is obtained:

$$\left(-\frac{1}{2}\sqrt{\frac{1}{R_o R_{mp}}}\right)\frac{R_{mp}}{f_s} + \left(1 - \sqrt{\frac{R_{mp}}{R_o}}\right)\frac{1}{f_s} = 0 \rightarrow 1 - \frac{3}{2}\sqrt{\frac{R_{mp}}{R_o}} = 0 \tag{20}$$

Therefore, by solving Equation (20) and replacing it in Equation (17), Equation (21) is obtained as follows:

$$\frac{R_{mp}}{R_o} = \frac{4}{9} \rightarrow L = \frac{1}{3}\frac{R_{mp}}{f_s} \tag{21}$$

2.2.3. Determining the duty cycle

The permissible duty cycle range is determined by assuming that the output voltage of the boost converter is constant and its current is continuous as given in Equation (22):

$$D = 1 - \frac{V_{mp}}{V_o} \rightarrow D_{min} = 1 - \frac{V_{mp}^{max}}{V_o}, D_{max} = 1 - \frac{V_{mp}^{min}}{V_o} \tag{22}$$

2.2.4. Sizing the input capacitor

The input capacitor is used to reduce the input fluctuations of the boost converter. This capacitor is placed in parallel with the solar cell. If the capacitor is not present, the current passing through the cell changes greatly with a small change in the cell voltage based on the characteristic curve, and the cell may be far away from the MPP [39]. If the voltage of the solar cell changes, the electric charge changes in the capacitor, and an opposite current is generated in the capacitor, which is obtained from Equation (23):

$$\Delta I_c = C_i \frac{\Delta V_{mp}}{\Delta t} \tag{23}$$

Hence, the size of the input capacitor is provided by Equation (24) [39]:

$$C_i = \frac{-\Delta I_L \Delta t}{\Delta V_{mp}} = -\left(\frac{D V_{mp}}{f_s L}\frac{\Delta t_1}{\Delta V_{mp}} + \frac{(1-D)(V_{mp} - V_o)}{f_s L}\frac{\Delta t_2}{\Delta V_{mp}}\right) \tag{24}$$

The current passing through the capacitor changes during two-time intervals of $\boldsymbol{\Delta t_1 = \frac{D}{f_s}}$ and $\boldsymbol{\Delta t_1 = \frac{1-D}{f_s}}$, so we have:

$$C_i = \left(\frac{DV_{mp}}{f_s L}\frac{D}{f_s \Delta V_{mp}} + \frac{(1-D)}{f_s L}\frac{DV_{mp}}{1-D}\frac{(1-D)}{f_s \Delta V_{mp}}\right) = \frac{DV_{mp}}{f_s^2 L \Delta V_{mp}} \quad (25)$$

in which the value of the switching frequency is known, so the value of the input capacitor will be the function of the duty cycle, the inductance of the inductor, and the voltage ripple of the solar cell [39].

2.2.5. Sizing the output capacitor

The output capacitor is determined to adjust the output voltage ripple. Usually, when the power switch is ON, the current of the output capacitor is discharged in the resistance, and therefore its voltage changes according to Equation (26):

$$C_o = \frac{DV_o}{fR_o \Delta V_o} \quad (26)$$

2.3. Model prediction control method

The use of MPPT with predictive control is presented in this paper. This is due to the fast dynamic response suitable for controlling this type of system. It can be easily implemented and included in all types of systems, nonlinear constraints and situations, and multivariable cases for control and with easy implementation. The desired behavior of the system is formulated. In this control scheme, the open-loop model is used to predict and select the desired excitation, which provides a predictive horizon for control feedback. This means that only the first element of the optimized excitation sequence is applied and the entire optimization is recalculated at the sampling period. The block diagram of the proposed predictive control system for the system under study is shown in Figure 4.

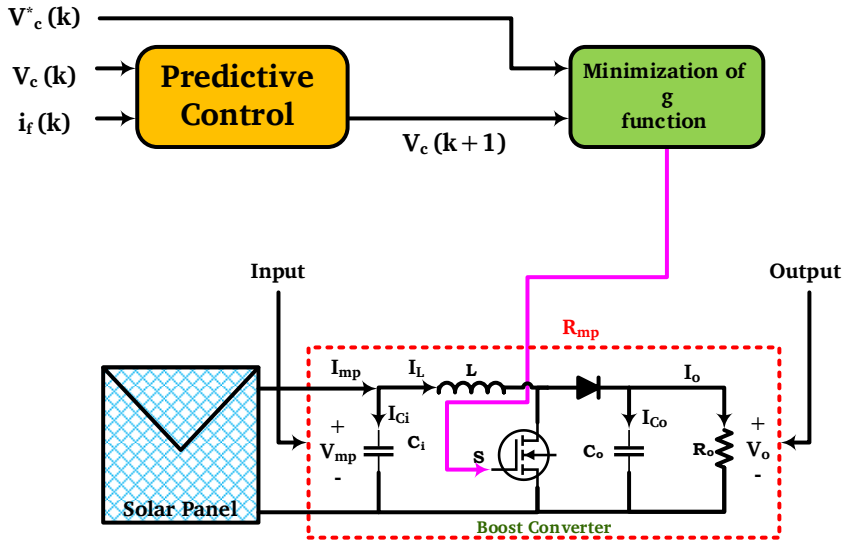

Figure 4. Block diagram of the prediction control [33].

The output voltage $v_c(k)$ and filter current $i_f(k)$ are measured for prediction by Equation (27) [33].

$$x(k+1) = A_q x(k) + B_q v_i(k) + B_{dq} i_o(k) \quad (27)$$

Where:

$$A_q = e^{AT_s}, B_q = \int_0^{Ts} e^{A\tau} B d\tau, and \quad B_{dq} = \int_0^{T_s} e^{A\tau} B_d d\tau. \quad (28)$$

The dynamic behavior of the output voltage can be stated as Equation (29):

$$C\frac{dv_c}{dt} = i_f - i_o \quad (29)$$

where C is the capacitor of the filter.

3. Case Study and Results

3.1. Case Study

The solar cell used in this study is a 50-W monocrystalline panel marketed under the brand name of MartSPM050-M. The specifications are presented in Table 1.

The maximum amount of irradiation in this study is 1000 W/m^2 and its minimum value is 200 W/m^2. Studies have been done with irradiances of 200, 400, 600, 800, and 1000 W/m^2.

3.2. Data of the boost converter

Some parameters are predetermined by the manufacturer or the standards before the design for designing the boost converter. These parameters play an important role in solving the problem. Table 2 presents the technical data required for designing the boost converter.

Table 1. The technical data of the studied PV cell [33].

Parameter	Symbol	Value	Dimension
Open-circuit voltage	V_{OC}	22.53	V
Short-circuit current	I_{SC}	2.97	A
MPP voltage	V_{mp}	18.68	V
MPP current	I_{mp}	2.77	A
Temperature coefficient of the open-circuit mode	K_v	-0.0789	Celsius/V
Temperature coefficient of the short-circuit mode	K_i	0.1485	Celsius/mA
Irradiance in standard conditions	G_{stc}	1000	W/m^2
Temperature in standard conditions	T_{stc}	25	Celsius degree
Boltzmann's constant	k	1.38×10^{-23}	Joule/Kelvin
Charge of an electron	q	1.6×10^{-19}	Coulomb

3.3. Simulation results

3.3.1. Extracting the characteristic curve of the PV cell

The characteristic curve of the solar cell is obtained by Equations (1) to (4) and according to the technical information mentioned in the datasheet of the solar cell (see Table 1). The current-voltage curve of the solar cell is shown in Figure 5. Also, Figure 6 depicts the voltage-power characteristic of the cell. The voltage-resistance characteristic of the solar cell is also depicted in Figure 7.

Table 2. The technical data required for designing the boost converter [33].

Parameter	Symbol	Value
Switching frequency of IGBT	f_s	20
Maximum ripple of the PV cell voltage	$\Delta V_{mp}/V_{mp}$	1
Maximum ripple of the converter output voltage	$\Delta V_o/V_o$	1
Maximum ripple of inductor current	$\Delta I_L/I_L$	15
Minimum allowable duty cycle	D_{min}	10
Maximum allowable duty cycle	D_{max}	60

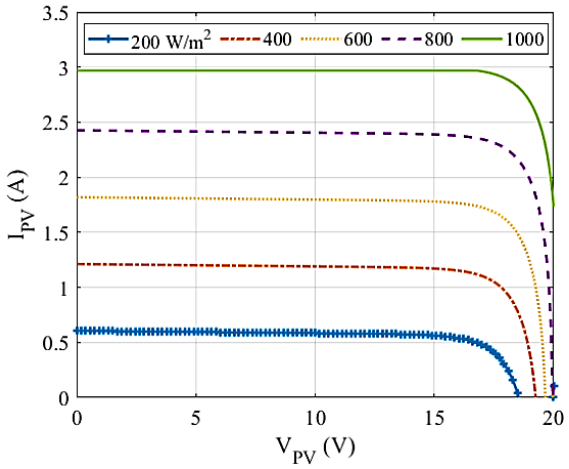

Figure 5. The V-I characteristic curve of the PV cell.

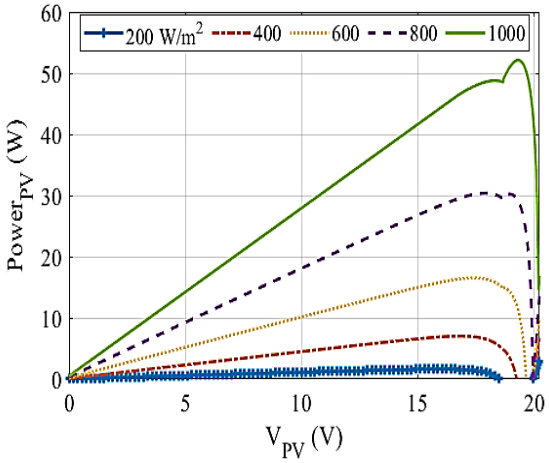

Figure 6. The V-P characteristic curve of the PV cell.

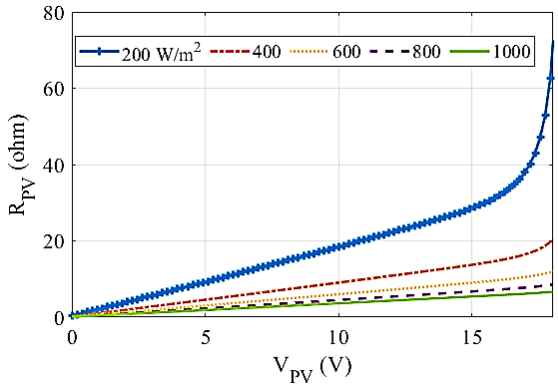

Figure 7. The V-R characteristic curve of the PV cell.

Figure 5 shows the dependence of PV behavior on irradiance. The graphs related to higher irradiation are placed on the top of the other graphs. This means that the higher the irradiation, the larger the short-circuit current. Also, the current corresponding to the MPP will increase. From the point of view of open-circuit voltage, irradiation does not greatly impact the results.

It is inferred from Figure 6 that with the increase of irradiation, the PV power curve is placed above the other graphs. This means that the ability to extract thermal energy has increased and it is possible to obtain more solar power. The voltage of the MPP does not express much changes, but the current supplied by PVs has increased due to irradiation, and as a result, the power has increased.

From the perspective of the equivalent resistance of the solar cell, it can be seen in Figure 7 that the increase in irradiation leads to a decrease in PV resistance, and the lowest amount of resistance belongs to the highest amount of solar radiation. Also, this resistance changes depending on the voltage at both ends of the panel and shows a strictly upward and exponential trend with respect to voltage changes. In order to transfer the maximum power to the load, the impedance must be adjusted and the PV operating point must be determined. These figures, especially Figure 7, give the minimum and maximum resistance values of the solar cell in different radiations. In this study, the minimum resistance of the solar cell is at the MPP, equal to $R_{mp}^{\min} = 6.62\Omega$, which belongs to the irradiation of 1000 W/m^2. The maximum resistance of a solar cell is $R_{mp}^{\max} = 29.87\Omega$, which belongs to the irradiation of 200 W/m^2.

Table 3. The results of designing the boost converter components under three different conditions.

Element	Constant R_o	Limitless R_o	R_o with a forced limit
Output resistance (Ω)	38.996	Rheostat from 8.1728 to 186.68	Rheostat from 8.1728 to 70
Output capacitor (μF)	75.39	111.90	111.90
Inductance (mH)	1.92	5.97	3.45
Input capacitor (μF)	9.54	3.14	3.14

3.3.2. Boost converter design using power control tracking

In this part of the simulation, the behavior of the designed converters is examined from two viewpoints, including:

Scenario 1: The constant output resistance, constant irradiation, and initial duty cycle value are set to 35%. By changing the constant-step duty cycle, the converter tries to track the power point using the HC method, without violating its allowed range.

Scenario 2: The output resistance is variable, the irradiation remains constant, and only the cell output voltage fluctuates by 10%, the constant-step duty cycle tries to adjust the output voltage of the boost converter.

To examine the above scenarios, it is necessary to implement them with MATLAB software. The Simulink toolbox was used to simulate this method. The circuit diagram of the implementation of this converter in MATLAB software is shown in Figure 8.

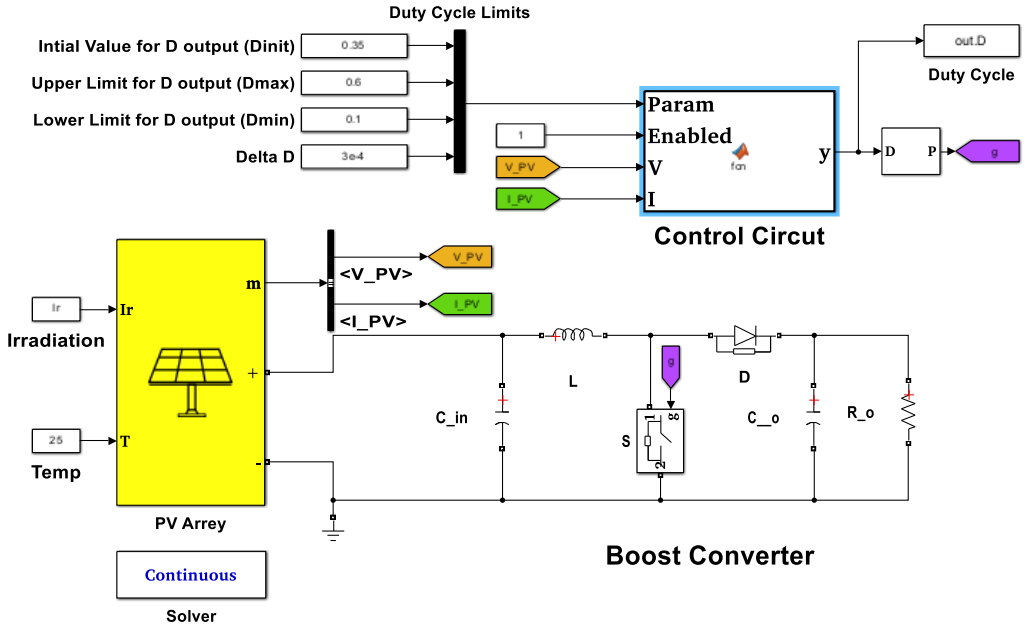

Figure 8. A schematic of the circuit implemented in the Simulink toolbox.

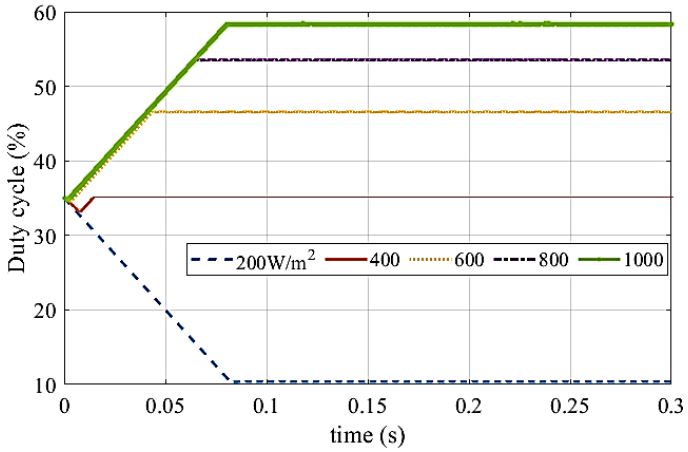

Figure 9. The performance of the power tracking system in achieving the MPP by adjusting the duty cycle at constant output resistance.

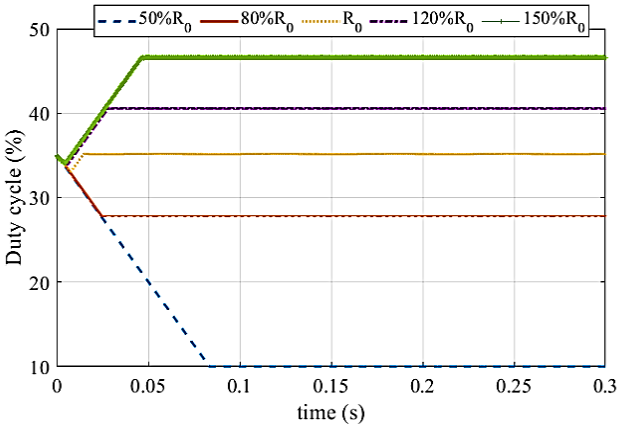

Figure 10. The effect of changing the output resistance (relative to the optimal value) for MPPT in the irradiation of 400 W/m^2.

The amount of radiation remains constant during each simulation, but the voltage of the solar cell and the current passing through it change, and the duty cycle must increase or decrease its value (with a constant step) based on the MPP. In the case that the resistance is constant, only the duty cycle can be effective in the results of the problem. Nonetheless, if the resistance is chosen as a rheostat, changing the resistance can also be used as an auxiliary solution.

Scenario 1 (constant output resistance): Figure 9 shows the performance of the power tracking system for different irradiations. The information about the inductor, capacitors, and output resistance is taken from the information in the first column of Table 3 and applied to the simulation.

Figure 10 illustrates well the result of the distance of the output resistance value from its optimal value. As is evident, the MPP is found faster in the selected optimal value than in other cases. As the distance from the optimal value increases, the time to reach the MPP also increases. The second remark is that changing the value of the output resistance has led to a change in the duty cycle. In the case of irradiation of 400 W/m^2, it can be seen that the duty cycle is not limited. Only if the output resistance is halved (striped blue), the tracking system reaches its limit and the solution will not be very acceptable. The third remark is that the less the irradiation, the higher the possibility of the system not being able to reach the duty cycle. The duty cycle limitation may lead to the lack of access to the correct solution. On the other hand, increasing the output resistance may cause the system to face a high duty cycle limit. Another factor indicating the correctness of the design of the proposed tracking system is examining the amount of input voltage ripple, inductor current ripple, and output voltage ripple in each of the MPPs obtained in the system, which is shown in Table 4.

Scenario 2 (variable output resistance): In this scenario, the output resistance is not constant and is designed based on the second column of Table 3 of circuit elements. The analysis of scenario 2 is also similar to scenario 1, with the difference that the results are not checked only in one output resistance but the justification of the system's behavior in a range of resistances from 8.17 to 186.68 Ω must be investigated. The ability of the system to find the MPP in different ranges of irradiation and output resistance is one of

the important issues. First of all, in the beginning, it should be determined what range of output resistance will be acceptable for each irradiation, and in that determined range, the tracking system can find the MPP suitably.

Table 4. Investigating the technical parameters of the MPP tracker converter in different irradiations (constant output resistance).

Irradiation (W/m²)	Resistance of solar cell	Input voltage ripple in the MPP (%)	Inductor current ripple in the MPP (%)	Output voltage ripple in the MPP (%)
200	32.38	0.2	10.0	0.2
400	16.61	0.63	14.88	0.63
600	11.18	0.79	13.93	0.79
800	8.40	0.93	11.95	0.93
1000	6.75	0.99	10.30	0.99

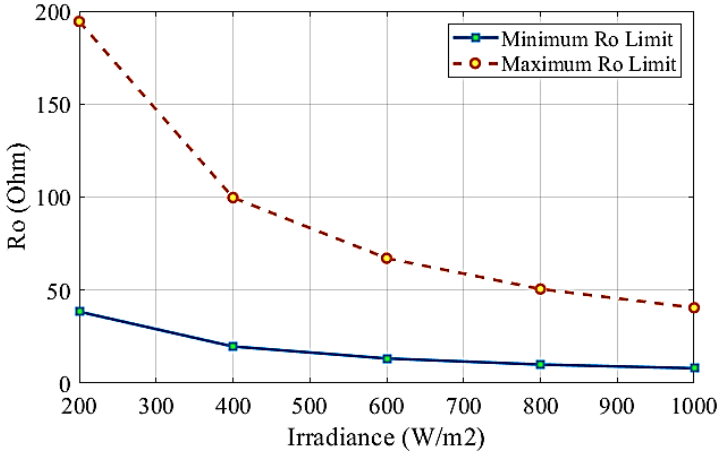

Figure 11. The permissible range of output resistance of the MPP tracker converter in different irradiations.

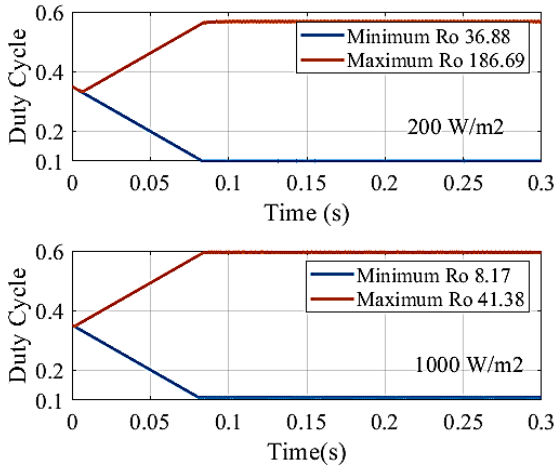

Figure 12. The duty cycle behavior in the upper and lower ranges of the output resistance for irradiations of (a) 200 W/m² and (b) 1000 W/m².

According to Figure 11, it can be concluded that firstly as the irradiation decreases, the minimum and maximum allowed value of the output resistance must increase and it will not be possible to reach the MPP in smaller resistances. The justification for this behavior is given in Equation (8). As it is clear in this equation, when the irradiation is low, the duty cycle needs to be higher to maintain the stability of the system, so the value of the output resistance will be larger. Secondly, the higher the radiation, the smaller the distance between the minimum and maximum allowed output resistance. In other words, the range of permissible variations of the output resistance will be lower. It is also possible to justify this according to Equations (10) to (13). It is clear in these relationships that with the increase in irradiation, the range of duty cycle variations decreases, so the range of output resistance variations becomes narrower. Another essential issue in Scenario 2 is specifying the range of duty cycle variations in each of the irradiations and output resistance limits determined in Figure 12, whose result is displayed in Figure 13.

The cycle should also be less than the allowed value, which will not be acceptable. Also, the higher the irradiation, the higher the duty cycle in a shorter period of time. Calculating the ripples of inductor current and input and output capacitor voltages is another important parameter in understanding the behavior of the power tracker converter, whose results are shown in Table 5. Analyzing the output voltage of the system in different irradiations and the resistance of different outputs is illustrated in Figure 13. According to Figure 11, larger resistances will bring the duty cycle closer to the maximum, and smaller resistances will bring the duty cycle closer to its lower limit.

Table 5. Variations in the ripple of the input voltage, output voltage, and inductor current for different resistances and irradiations.

Irradiation (W/m^2)	Output resistance	Input voltage ripple in the MPP (%)	Inductor current ripple in the MPP (%)	Output voltage ripple in the MPP (%)
200	37.300	0.182	0.529	0.113
	49.734	0.401	4.381	0.180
	73.890	0.558	8.269	0.215
	88.810	0.668	9.897	0.214
	105.151	0.829	11.232	0.191
	131.439	0.872	12.897	0.176
	150.266	0.921	13.811	0.165
	165.543	0.963	14.434	0.158
	8.171	0.215	0.470	0.681
1000	14.920	0.3765	2.001	1.001
	25.222	0.533	2.325	0.810
	38.011	0.803	3.547	0.672

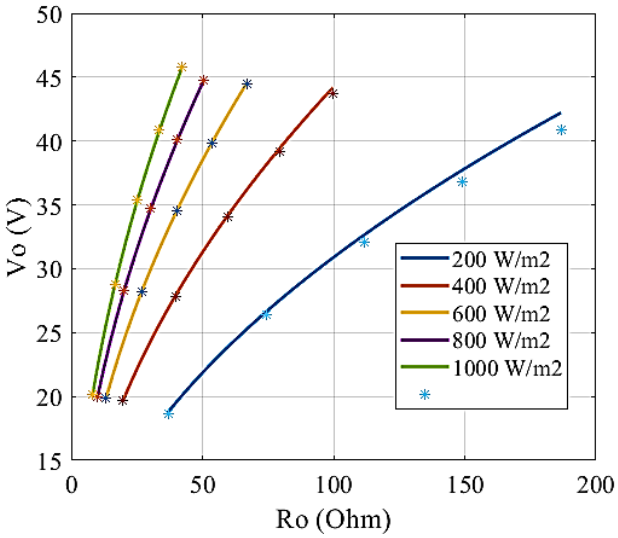

Figure 13. The behavior of the output voltage in different irradiations and output resistances.

4. Conclusions

It can be concluded that the proposed power tracker converter could find the MPP within the designed range of the output resistance so that the duty cycle did not violate its predetermined range. Also, the MPP was found to be highly dependent on the solar irradiance, and since the step related to tracking the power in this method was assumed to be constant, the system tracks the MPP very quickly around irradiation amounts of 400 to 600 W/m2. However, the time to reach the MPP will be longer as the irradiation value deviates further from this range. Moreover, the higher the output resistance, the greater the tendency of the tracking system to move towards larger duty cycles to track the MPP. As the resistance decreases from the optimal value, the duty cycle will move towards its minimum value. The designs showed that the proposed method would lead to maintaining the ripples in the input capacitor voltage, output capacitor voltage, and inductor current within their allowed range. The results demonstrated that the variable resistance method worked in a wider working range than the constant resistance method. Therefore, it would have a more comprehensive performance. Nevertheless, the computational burden of the constant resistance method was less. This method can be used as a simple method for PV energy management. The simulation effects demonstrated the efficacy of the proposed technique in attaining the objectives. The counseled technique can correctly song the MPP inside a vast spectrum of solar radiation while ensuring that the duty cycle remains inside its permissible variety.

References

[1] Z. Ishrat, A. K. Gupta, and S. Nayak, "A Comprehensive Review of MPPT Techniques Based on ML Applicable for Maximum Power in Solar Power Systems," *Journal of Renewable Energy and Environment*, vol. 11, no. 1, pp. 28-37, 2024.

[2] M. Abasi, M. F. Nezhadaneini, M. Karimi, and N. Yousefi, "A Novel Metaheuristic Approach to Solve Unit Commitment Problem in the Presence of Wind Farms," *Rev Roumaine des Sciences Techniques-Series Electrotechnique et Energetique*, vol. 60, no. 3, pp. 253-262, 2015.

[3] K. Fatima, A. F. Minai, and H. Malik, "Intelligent Approach-Based Maximum Power Point Tracking for Renewable Energy System: A Review," *Intelligent Data Analytics for Power and Energy Systems*, pp. 373-405, 2022.
[4] A. G. Abo-Khalil, I. I. El-Sharkawy, A. Radwan, and S. Memon, "Influence of a Hybrid MPPT Technique, SA-P&O, on PV System Performance Under Partial Shading Conditions," *Energies*, vol. 16, no. 2, p.577, 2023.
[5] A. G. Abo-Khalil, K. Sayed, A. Radwan, and I. A. El-Sharkawy, "Analysis of the PV System Sizing and Economic Feasibility Study in a Grid-Connected PV System," *Case Studies in Thermal Engineering*, vol. 45, 102903, 2023.
[6] M. H. Ibrahim, S. P. Ang, et al., "Optimizing Step-Size of Perturb & Observe and Incremental Conductance MPPT Techniques Using PSO for Grid-Tied PV System," *IEEE Access*, vol. 11, pp. 13079-13090, 2023.
[7] L. Gong, G. Hou, and C. Huang, "A Two-Stage Mppt Controller For Pv System Based on the Improved Artificial Bee Colony and Simultaneous Heat Transfer Search Algorithm," *ISA transactions*, vol. 132, pp. 428-443, 2023.
[8] A. Refaat, Q. A. Ali, et al., "Extraction of Maximum Power From PV System Based on Horse Herd Optimization MPPT Technique Under Various Weather Conditions," *Renewable Energy*, vol. 220, 119718, 2024.
[9] M. Sadeghi, and M. Abasi, "Optimal Placement and Sizing of Hybrid Superconducting Fault Current Limiter for Protection Coordination Restoration of the Distribution Networks in the Presence of Simultaneous Distributed Generation," *Electric Power Systems Research*, vol. 201, 107541, 2021.
[10] M. Abasi, M. Joorabian, A. Saffarian, and S.G. Seifossadat, "A Comprehensive Review of Various Fault Location Methods for Transmission Lines Compensated by FACTS Devices and Series Capacitors," *Journal of Operation and Automation in Power Engineering*, vol. 9, no. 3, pp. 213-225, 2021.
[11] F. Rebert, and W. Gerold, "*Modular Series on Solid State Devices*," Addison-Wesley Publishing Company, vol. I, 1983.
[12] G. N. Tiwari, and S. Dubey, *"Fundamentals of Photovoltaic Modules and Their Applications*," Royal Society of Chemistry, 2009.
[13] L. M. Carrasco, F. J. Martín-Campo, L. Narvarte, M. T. Ortuño, and B. Vitoriano, "Design of Maintenance Structures for Rural Electrification with Solar Home Systems. The Case of the Moroccan Program," *Energy*, vol. 117, pp. 47-57, 2016.
[14] Y. Fan and X. Xia, "A Multi-Objective Optimization Model for Energy-Efficiency Building Envelope Retrofitting Plan with Rooftop PV System Installation and Maintenance," *Applied Energy*, vol. 189, pp. 327-335, 2017.
[15] F. Spertino, and F. Corona, "Monitoring and Checking of Performance in Photovoltaic Plants: A Tool for Design, Installation and Maintenance of Grid-Connected Systems," *Renewable Energy*, vol. 60, pp. 722-732, 2013.
[16] Y. Yu, G. Konstantinou, B. Hredzak, and V. G. Agelidis, "Operation of Cascaded H-Bridge Multilevel Converters for Large-Scale Photovoltaic Power Plants Under Bridge Failures," *IEEE Transactions on Industrial Electronics*, vol. 62, no. 11, pp. 7228-7236, 2015.
[17] X. Hu, and C. Gong, "A High Gain Input-Parallel Output-Series DC/DC Converter with Dual Coupled Inductors," *IEEE Transactions on Power Electronics*, vol. 30, no. 3, pp. 1306-1317, 2014.
[18] M. S. Bhaskar, S. Padmanaban, and F. Blaabjerg, "A Multistage DC-DC Step-Up Self-Balanced and Magnetic Component-Free Converter for Photovoltaic Applications Hardware Implementation," *Energies*, vol. 10, no. 5, 2017.
[19] T. Duman, S. Marti, M. A. Moonem, A. A. R. Abdul Kader, and H. Krishnaswami, "A Modular Multilevel Converter with Power Mismatch Control for Grid-Connected Photovoltaic Systems," *Energies*, vol. 10, no. 5, 2017.
[20] D. Zhao, M. Qian, J. Ma, and K. Yamashita, "Photovoltaic generator model for power system dynamic studies," *Solar Energy*, vol. 210, pp. 101-114, 2020.
[21] H. Meng, X. Ye, et al., "Equivalent Modeling and Simulation for PV System on Dynamic Clustering Equivalent Strategy," *IECON 2017-43rd Annual Conference of the IEEE Industrial Electronics Society*, pp. 5779-5784, 2017.

[22] S. M. MacAlpine, "Characterization and Capture of Photovoltaic System Losses Due to Nonuniform Conditions," Doctoral dissertation, University of Colorado at Boulder, 2014.
[23] M. Hejri, H. Mokhtari, M. R. Azizian, M. Ghandhari, and L. Söder, "On the Parameter Extraction of a Five-Parameter Double-Diode Model of Photovoltaic Cells and Modules," *IEEE Journal of Photovoltaics*, vol. 4, no. 3, pp. 915-923, 2014.
[24] D. L. King, J. A. Kratochvil, and W. E. Boyson, "Photovoltaic Array Performance Model," United States. Department of Energy, 2004, Vol. 8, pp. 1-19.
[25] A. Y. Abdelaziz, and Y. Almoataz, *Modern Maximum Power Point Tracking Techniques for Photovoltaic Energy Systems*. Springer Nature Switzerland AG, 2020.
[26] K. Ishaque, and Z. Salam, "A Review of Maximum Power Point Tracking Techniques of PV System for Uniform Insolation and Partial Shading Condition," *Renewable and Sustainable Energy Reviews*, vol. 19, pp. 475-488, 2013.
[27] B. Nayak, A. Mohapatra, and K. B. Mohanty, "Selection Criteria of DC-DC Converter and Control Variable for MPPT of PV System Utilized in Heating and Cooking Applications," *Cogent Engineering*, vol. 4, no. 1, p. 1363357, 2017.
[28] J. M. Enrique, E. Duran, M. Sidrach-de-Cardona, and J. M. Andujar, "Theoretical Assessment of the Maximum Power Point Tracking Efficiency of Photovoltaic Facilities with Different Converter Topologies," *Solar Energy*, vol. 81, no. 1, pp. 31-38, 2007.
[29] K. Dubey, and M. T. Shah, "Design and Simulation of Solar PV System," *2016 International Conference on Automatic Control and Dynamic Optimization Techniques (ICACDOT)*, pp. 568-573, IEEE, 2016.
[30] N. Chatrenour, H. Razmi, and H. Doagou-Mojarrad, "Improved Double Integral Sliding Mode MPPT Controller-Based Parameter Estimation for a Stand-Alone Photovoltaic System," *Energy Conversion and Management*, vol. 139, pp. 97-109, 2017.
[31] R. Ayop, and C. W. Tan, "Design of Boost Converter Based on Maximum Power Point Resistance for Photovoltaic Applications," *Solar Energy*, vol. 160, pp. 322-335, 2018.
[32] A. Dehghanzadeh, G. Farahani, H. Vahedi, and K. Al-Haddad, "Model Predictive Control Design for DC-DC Converters Applied to a Photovoltaic System," *International Journal of Electrical Power & Energy Systems*, vol. 103, pp. 537-544, 2018.
[33] E. Irmak, and N. Güler, "A Model Predictive Control-Based Hybrid MPPT Method for Boost Converters," *International Journal of Electronics*, vol. 107, no. 1, pp. 1-16, 2019.
[34] M. Mosa, H. A. Rub, M. E. Ahmed, and J. Rodriguez, "Modified MPPT with Using Model Predictive Control for Multilevel Boost Converter," *IECON 2012-38th Annual Conference on IEEE Industrial Electronics Society*, IEEE, pp. 5080-5085, 2012.
[35] M. Metry, S. Bayhan, M. B. Shadmand, R. S. Balog, and H. A. Rub, "Sensorless Current Model Predictive Control for Maximum Power Point Tracking of Single-Phase Submultilevel Inverter for Photovoltaic Systems," *Energy Conversion Congress and Exposition (ECCE)*, pp. 1-8, IEEE, 2016.
[36] M. Abedini, R. Eskandari, J. Ebrahimi, M. H. Zeinali, and A. Alahyari, "Optimal Placement of Power Switches on Malayer Practical Feeder to Improve System Reliability Using Hybrid Particle Swarm Optimization with Sinusoidal and Cosine Acceleration Coefficients," *Computational Intelligence in Electrical Engineering*, vol. 11, no. 2, pp.73-86, 2020.
[37] E. Chegeni, M. Zandieh, and J. Ebrahimi, "Attitude Control of Satellite with Pulse-Width Pulse-Frequency (PWPF) Modulator Using Generalized Incremental Predictive Control," *Majlesi Journal of Electrical Engineering*, vol. 8, no. 3, pp. 25-31, 2014.
[38] H. Makvandi, M. Abasi, et al., "Design of an Optimal STATCOM Controller to Enhance Dynamic Stability of the Smart Grid," *27th International Electrical Power Distribution Networks Conference (EPDC)*, pp. 94-101, IEEE, 2023.
[39] H. Makvandi, M. Abasi, et al., "Design of New Intelligent Islanding Detection Scheme in Multi-Machine Power Systems to Prevent Wide-Area Blackouts," *12th Smart Grid Conference (SGC)*, pp. 1-7, IEEE, 2022.

Declaration of Competing Interest

The authors declare that they have no known competing financial interests or personal relationships that could have appeared to influence the work reported in this paper. The ethical issues, including plagiarism, informed consent, misconduct, data fabrication and/or falsification, double publication and/or submission, redundancy, have been completely observed by the authors.

Credit Authorship Contribution Statement

Moaiad Mohseni: Conceptualization, Formal analysis, Project administration, Supervision, Validation, Roles/Writing - original draft. **Alireza Niknam Kumleh:** Conceptualization, Investigation, Methodology, Resources, Visualization, Writing - review & editing. **Mehdi Alibakhshi**: Methodology, Resources, Software, Supervision, Validation. **Mona Sheikhi Abou Masoudi:** Funding acquisition, Investigation, Writing-review & editing.

Bibliography

Moaiad Mohseni was born in Kwait. He received his B.SC Degree in Electrical Engineering, Kazeroon Branch, Islamic Azad University, Kazeroon, Iran in 2001, and his M.S. and Ph.D. degrees in Electrical Engineering from Dezful Branch, Islamic Azad University, Dezful, Iran, in 2011and 2021, respectively. His Research Include Power Market and Smart Grid and renewable energy systems.

Alireza Niknam Kumleh was born in Tehran. He received his B.SC Degree in Electrical Engineering, Faculty of Electrical Engineering, Amirkabir University of Technology (Tehran polytechnic), Tehran, Iran in 2012, and his M.S. degrees in Electrical Engineering from Faculty of Electrical Engineering, Amirkabir University of Technology (Tehran polytechnic), Tehran, Iran in 2015, respectively. His Research Include Power Market, Smart Grid, renewable energy systems.

Mehdi Alibakhshi was born in Iran in 1985. He received his Master degree in control engineering from south Tehran Branch, Islamic Azad University, Tehran, Iran, in 2011. He currently works as a researcher. Also, he has taught for ten years at Borujerd Islamic Azad University. he has published one research papers, one conference papers. His research interests include power electronic, predictive control, and microgrids.

Mona Sheikhi Abou Masoudi was born in Iran in 1986. She received his Master degree in Electronic Engineering from Oloom Tahghighat Branch, Islamic Azad University, Tehran, Iran, in 2011. She currently works as a teacher in Naghshe Jahan institute. Also, she has taught for ten years at Sepahan and Safahan and Kharazmi university. She has published two research papers, one conference papers. Her research interests include power electronic, control, and microgrids.